Meridional circulation in the western coastal zone:

II. The regulation by pressure gradient set up through basin scale circulation and the western boundary current transport

Qinyan Liu[+$] & Rui Xin Huang[+*]

[+] South China Sea Institute of Oceanology, Chinese Academy of Sciences, Guangzhou, China

[*] Woods Hole Oceanographic Institution, Woods Hole, MA 02543, USA

February 2, 2010

Will be submitted to *J. Phys. Oceanography*

[$] Corresponding author: Qinyan Liu, South China Sea Institute of Oceanology, Chinese Academy of Sciences, Guangzhou, China, qyliu66@scsio.ac.cn

Abstract

The circulation in the western coastal regime is conceptually treated as a boundary layer attached to the basin-scale circulation. Accordingly, the meridional pressure gradient along the outer edge of the coastal zone is set up by the zonal integration of the zonal wind in the basin interior. Scaling analysis indicates that this meridional pressure gradient is much larger than the local meridional wind stress. Although the meridional pressure gradient may be attenuated toward the shore, over a major portion of the coastal zone it is a dominating driving force regulating the circulation. Analysis of results obtained from a numerical model shows that on interannual/decadal time scale, the meridional transport of the coastal circulation is highly correlated to both this meridional pressure gradient and the western boundary current transport. Thus, the meridional pressure gradient set up by the wind-driven gyre along the outer edge of the coastal zone can be used as an index for analyzing changes of coastal circulation on interannual/decadal time scales.

1. Introduction

In Part I of this study (Huang and Liu, manuscript), we have demonstrated that to a large degree, the meridional current in the western coastal zone is subject to a meridional pressure gradient set up by the basin-scale wind-driven circulation. In this part, the coastal circulation is treated as a boundary layer attached to the interior solution and the western boundary current. The focus is on the barotropic circulation in the coastal zone which is primarily driven by wind stress, thus we will treat the circulation in terms of a single-layer model and omit the baroclinic circulation associated with thermohaline forcing.

Oceanic circulation in the coastal region and the open ocean has many different dynamical features; thus, in the traditional way, circulation in the ocean is separated into the large-scale circulation in the basin interior and the circulation in the coastal area. Due to historic reasons, including the limitation of computer power, coastal circulation has been mostly studied as a system more or less separated from the open ocean. The interaction between the open ocean and the coastal ocean involves complicated phenomena. It seems that a major dynamical barrier for the interaction between the open ocean and the coastal ocean exists, e.g., Brink (1998). In order to understand this interaction we must find a way to break this barrier.

There are coastal currents in the Chinese marginal seas which flow against local wind, so that the dynamical mechanisms maintaining such currents have long been a puzzle. For example, there is a nearly permanent northward flow through the Taiwan

Strait (the Taiwan Strait Warm Current, TSWC hereafter), which is against the local wind stress, e.g., Guan and Chen (1964), Guan (2002), Guan and Fang (2006). The possible mechanisms have long been speculated, such as the study of Chuang (1986). In particular, he postulated that "A pressure gradient at the southern end of the strait seems to be the only plausible mechanism", although no detailed analysis was outlined.

Recent study by Yang (2007) has been focused on the role played by the Kuroshio transport. According to his argument, the pressure difference between the southern and northern parts of the strait is set by friction associated with Kuroshio. This point is similar with Chuang (1986), and the alongshore coastal sea level slope is attributed mainly as a feature induced by Kuroshio branching. We postulate that the meridional pressure gradient can be linked to the meridional gradient of zonal wind stress integrated from the western boundary to the eastern boundary. Although our approach and Yang's approach are dynamically linked, our scheme leads a simple index which can be used to explore the variability of the TSWC on interannual to decadal time scales.

As in many applications of boundary layer theory, the along-stream pressure gradient is primarily set up by the circulation outside the coastal zone. Due to strong dynamical processes taking place within the coastal area, such as bottom friction and the nonlinear interaction, the meridional pressure gradient imposed by the gyre-scale circulation at the outer edge of the coastal zone may be heavily attenuated. The exact distribution of the meridional pressure gradient over the coastal zone is hard to

describe in terms of a simple model. Thus, we will use the meridional pressure gradient at the outer edge of the coastal zone set up the basin-interior wind-driven circulation as an index for studying the meridional circulation over the coastal zone. Whether such an index is useful or not will be verified through analyzing results obtained from a numerical model building with more complete dynamic constraints.

Therefore, the coastal circulation in the along-shore direction is the outcome of the competition between the along-shore pressure gradient set up by basin-scale circulation and the local wind stress. Coastal circulation is subject to the decadal variability of wind stress in the basin interior. As shown in part I, under time-varying wind stress the variability of the western boundary current transport is quite different from that of the meridional pressure gradient at the outer edge of the coastal zone. Thus, including the Kuroshio or Gulf Stream in a coastal model may not be enough for the model to accurate simulating the coastal circulation.

We emphasize that the connection between the open ocean and the coastal ocean through the meridional pressure coupling is only one aspect of complicated interactions between the coastal ocean and the open ocean. Due to the limitation of computer power and other technical issues, open boundary conditions have been widely used in coastal ocean study. Although such open boundary conditions have been mathematically proved to be solid, they may not be able to simulate the complicated physical communication between the open ocean and the coastal circulation.

Over the past decades, a major new development in oceanic circulation theory is the recognition of the vital role of external sources of mechanical energy in maintaining/regulating the circulation. For the study of costal circulation it is important to include the dynamical role of the open ocean, such as the. Obviously, communication/exchange of mechanical energy from tides and wind stress, the momentum and pressure signals between the open ocean and the coastal zone is a key issue which affects the costal circulation, as shown in Fig. 1. It is clear that the traditional open boundary conditions are incapable in dealing with the transform of such dynamical information.

This study is organized as follows. In Section 2, we will discuss the meridional momentum balance in the coastal zone. Use scaling, we will show that the meridional pressure gradient set up by the basin scale zonal wind stress is the dominant driving force. In Section 3, this simple index will be applied to both the North Pacific Ocean and North Atlantic Ocean. In Section 4, we will apply this index to the study of the Chinese marginal seas, including the Taiwan Strait. Finally, we conclude in Section 5.

2. Meridional circulation in the coastal zone

We will separate the basin into two parts: the open ocean and the coastal ocean, as shown in Fig. 2. As discussed above, circulation in the open ocean can be described in terms of a reduced gravity model. The basin scale circulation sets up the meridional pressure gradient along the edge of the ‘western wall’, which is depicted by the short

vertical lines in Fig. 2. In the left part of Fig. 2, the ocean is classified as the coastal circulation, with a depth of *h*, which is much smaller than *H*, the depth of the main thermocline in the open ocean. Although the continental slope is relatively steep, it is not a vertical wall. However, for simplicity of the analysis, we will treat the western boundary of the model basin as a meridional and vertical wall. The general case with a non-meridional western boundary and a sloping continental slope is left for further study.

Over the coastal ocean, the corresponding y-momentum equation is in the following form

$$v_t + uv_x + vv_y + fu = -p_y / \rho_0 + \tau^y / \rho_0 h + \kappa v / \rho_0 h + A\nabla^2 v / \rho_0 h \qquad (1)$$

where κ is the bottom frictional parameter, and A is the horizontal friction parameter, and other forms of friction parameterization may be used as well. Since the coastal current is quite narrow compared with the basin-scale circulation, we assume that meridional pressure gradient within the coastal current is basically set up by the large-scale circulation. As discussed in Part I, within the framework of a reduced gravity model, the meridional pressure gradient over the coastal zone is approximately the same as that along the outer edge of the coastal zone, and the late terms is linked to the meridional gradient of the zonal integration of zonal wind stress, i.e.,

$$-\frac{1}{\rho_0}\frac{\partial p}{\partial y} \sim -\frac{1}{\rho_0 H}\int_{x_w}^{x_e}\frac{\partial \tau^x}{\partial y}dx\,. \qquad (2)$$

We adapt the common practice of the boundary layer theory and assume change in cross-shore direction of the meridional pressure gradient term is negligible. Instead of show the validity of such a bold assumption from the theoretical point, we will treat this as an index and leave the validation of many approximations to the section where we will verify the usefulness of this index through comparison with numerical model data assimilation.

Thus, the forces drive the coastal circulation are due to the large-scale pressure gradient force set up by the basin-scale circulation and the local meridional wind stress. The ratio of these two terms can be estimated through the following scaling

$$R = \frac{\left|\tau^y_{shelf}\right| / h}{\left|\frac{1}{\rho_0}\frac{\partial p}{\partial y}\right|} \sim \frac{\left|\tau^y_{shelf}\right| / h}{\left|\frac{1}{H}\int_{x_w}^{x_e}\frac{\partial}{\partial y}\tau^x dx\right|} = \frac{H}{h}\frac{\left|\tau^y_{shelf}\right|}{\left|\int_{x_w}^{x_e}\frac{\partial}{\partial y}\tau^x dx\right|}. \quad (3)$$

where τ^y_{shelf} denotes the meridional wind stress over the continental shelf. Thus, scaling analysis leads to

$$R \sim \frac{H}{h}\frac{L_y}{L_x}\left|\frac{\tau^y_{shelf}}{\tau^x}\right| \ll O(1). \quad (4)$$

In general, zonal wind stress is larger than the meridional wind stress, $\left|\tau^y_{shelf}\right| \approx (0.5-0.8)\left|\tau^x\right|$. For the Pacific basin, $L_y / L_x \approx 0.2$; thus, R is much smaller than one, i.e., the meridional pressure gradient along the outer edge of the coastal zone set up by basin scale wind-driven circulation overpowers that local meridional wind stress.

Of course, near the coastal line, the water is very shallow, and the small depth ratio gives rise to a relatively large R, i.e., within the shallow marginal sea the local meridional wind stress can play the role of regulating the meridional flow.

To compare the importance of contribution due to the basin-scale pressure force and the local meridional wind stress, we introduce the following index

$$F = -\alpha P_y + \tau^y_{shelf} \qquad (5)$$

where $\alpha = h / H$ is the ratio of layer thickness of the coastal ocean and the main thermocline along the outer edge of the wind-driven gyre. To demonstrate the basic balance, the wind stress data from the period of Jan. 1958 to Dec. 2007, taken from the recent release of SODA 2007 (http://dsrs.atmos.umd.edu/DATA) will be used.

We emphasize that our approach is directly linked to the traditional Island Rule, but with a slightly different method. The Island rule is based on the integration of wind stress along the whole loop as shown in Fig. 1, including the wind stress integration along the two meridional branches. Our method is to separate the contribution from the two line integrals of the zonal wind and that from the local meridional wind over the strait. Furthermore, we assume that the thermocline depth along the eastern boundary remains constant, and the integration of meridional wind stress along the eastern boundary of the basin is omitted. In addition, the contribution of topography is included in our approach in terms of the layer depth h in the coastal zone and the main thermocline depth H along the “western wall” of the basin-scale circulation.

Most importantly, our approach is aimed at the inviscid part of the basin-scale circulation outside the thin frictional boundary layer immediately adjacent to the island. Theory involved with such a frictional boundary layer is much more complicated than the corresponding inviscid flow region outside of this thin boundary layer discussed in may previous studies. Therefore, our approach can provide a much simpler dynamical picture, which can be used for our understanding of the regulation of the coastal circulation by basin-scale wind-driven circulation on interannual to decadal time scale.

3. Competition of forces driving the coastal meridional flow

According to Eq. (1), the meridional flow is driven by two forces, including the meridional pressure gradient and the local zonal wind stress; the other three forces also regulate the meridional flows, but their roles are passive. Although the meridional pressure gradient along the outer edge of the coastal zone set up by the wind-driven circulation in the basin interior is attenuated in the cross-shore direction, it remains a major regulator of the meridional circulation over the coastal zone. In order to demonstrate the dominating role of the meridional pressure gradient term set up by the basin scale wind stress we analyzed the wind stress data for both the North Pacific and North Atlantic oceans. The meridional pressure gradient term, labeled by $-P_y$, is calculated from Eq. (2), i.e., it is calculated from the meridional gradient of the basin-scale zonal wind stress integrated from the eastern boundary to the western boundary. The meridional wind stress, labeled by τ^y, is taken as the mean of the 5

zonal grids adjacent to the western boundary. The western boundary is defined as the place where the maximum meridional surface ocean current occurs.

Since the geometry of the subpolar basin is much more complicated, we will confine our discussion here to the subtropical basin and the related coastal circulation. Due to the difference in geometry, our study of these two oceans covers different meridional domains. In the Pacific Ocean, our calculation starts from 14^{o}N to 36^{o}N, but in the Atlantic Ocean, our model domain covers 24^{o}N to 40^{o}N.

The maximal depth of the main thermocline in the North Pacific Ocean is approximately 500-600 m; and the corresponding maximum depth in the North Atlantic Ocean is approximately 800 m (Part I). Assume the mean depth of the coastal ocean $h = 100m$; and the mean depth of main thermocline depth $H = 400m$ in Pacific and $H = 600m$ in Atlantic, then the mean $\alpha = 0.25$ and 0.15 respectively.

For the period of 1958-2007, basin-scale pressure gradient term along the western boundary in the Northern Pacific Ocean is poleward over the whole meridional domain, except at the southern end of the domain of concern (approximately south of 15^{o}N), left panel of Fig. 3. On the other hand, the meridional wind stress over the coastal zone is equatorward, right panel of Fig. 3. Most importantly, the meridional pressure gradient term is one order of magnitude larger than the local meridional wind stress, although its amplitude is reduced with $\alpha = 0.25$ (middle panel of Fig. 3). Therefore, the meridional flow is primarily dominated by the meridional pressure gradient set up by the basin-scale zonal wind stress, and a northward

counter-local-wind coastal transport is expected for this latitudinal band. In addition, the meridional pressure gradient diagnosed from the basin-scale zonal wind stress indicates a strong decadal variability. Such a variation of pressure force must have profound influence of the coastal circulation over the decadal time scale.

In the North Atlantic basin, the situation south of 38^{o}N is quite similar to that in the North Pacific Ocean, i.e., the local meridional wind stress over the coastal zone is mostly equatorward, and it is approximately one order of magnitude smaller than the pressure gradient term build up by the basin-scale zonal wind stress (right & left panels, Fig. 4). After the alpha is added, the role played by the pressure gradient term is also can overcome the local wind forcing, and induce a net flow along the pressure gradient (middle panel, Fig. 4).

A major difference between Fig. 3 and Fig. 4 is that the meridional domain in Fig. 4 covers a small portion of the subpolar basin where the strength of the westerly declines poleward. As a result, the pressure gradient term is negative over the latitude band north of 37^{o}N. Such a negative pressure gradient term should drive an equatorward flow in the corresponding latitudinal band in the coastal zone of the North American continent. In fact, filed observations indicate that there is a steady south-westward circulation over the continental rise at the 70^{o}W section for the latitude band of 38^{o}N-39^{o}N (Luyten, 1977). Csanady (1977) pointed out that this flow is linked with the long-shore slope of sea level, i.e. the long-shore pressure gradient force. However, our study here is focused on the coastal circulation along the eastern

coast of Asia; due to the limitation of space we will leave the detailed discussion of the coastal circulation in the North American eastern coast for further study.

4. Application of the index to the Chinese marginal seas

The winter counter-wind-current off the Southeast China Coast is an outstanding example of current flowing against the local wind stress firstly acknowledged by Guan and Chen (1964), which includes the South China Sea Warm Current (SCSWC), Taiwan Strait Warm Current (TSWC) and Taiwan Warm Current (TWC). These currents have been studied by in many previous publications, in particular the review presented by Guan (2002); Guan and Fang (2006). Based on previous studies, the basic characters and possible mechanisms regulating such counter-wind current were discussed.

The northward current in the Taiwan Strait might be treated as an extension of SCSWC, which is thought to be guided by the continental slope (Su and Wang, 1987). Recently, the important role of the meridional pressure gradient force in setting up the TSWC has been examined in light of the large-scale circulation environment. In particular, Yang (2007) pointed out the capital importance of the meridional pressure gradient set up by circulation around the Taiwan Island. Other recent publications by Yang and his colleagues further illustrated this critical issue through its leading role in regulating sea level variability along the west coast of Japan (Ma et al., 2009).

In this section, we will extend Yang's idea and explore the dynamical role of the meridional pressure force in details. In particular, we will find out how this

meridional pressure gradient force is linked to the basin-scale zonal wind stress for interannual to decadal time scales, and how important is this pressure term in comparison with the local meridional wind stress.

In order to illustrate our point, we selected two sections for monitoring the volume transport, including the Taiwan Strait Current along Section A (117.75 ^{o}E-120.75^{o}E, 24.25^{o}N) and Taiwan Warm Current off coast along Section B (124.25^{o}E-126.25^{o}E, 28.75^{o}N), Fig. 5.

The estimate the net force term F requires the specification of the layer thickness ratio for the coastal ocean and the main thermocline along the outer edge of the wind-driven gyre. The main thermocline along the outer edge of the wind-driven gyre (H) can be identified through an isothermal surface going through the core of the main thermocline, and for the present case, we use 14°C isotherm, whose depth can be used as a good proxy for the main thermocline in this part of the subtropical gyre. The layer thickness of the coastal ocean (h) is set to be a constant.

According the mean temperature profiles along 24.25^{o}N and 28.75^{o}N shown in Fig. 6, rough estimations of h and H can be made. The water depth of Taiwan Strait is mostly shallower than 100m combining the topography shown in Fig. 5, and then the layer thickness here is set to 100m. Along 28.75^{o}N, the layer thickness of the coastal ocean is set to 112.3m, which is the maximum ocean depth resolved by SODA datasets. The corresponding depth of the main thermocline depth is defined by the

depth of 14°C isotherm at station (123.25^{o}E, 24.25^{o}N) and (128.25^{o}E, 28.75^{o}N) respectively.

In climatologically mean, the 14°C isotherm depth at station (123.25^{o}E, 24.25^{o}N) is approximately 361.5m, and it is approximately 350.2m at station (128.25^{o}E, 28.75^{o}N). The thermocline depth along the outer edge of the wind-driven gyre identified from these two stations has a relatively small amplitude seasonal cycle, as shown in Fig. 7. In fact, our analysis shows that the thermocline depth in the open ocean has a positive seasonal anomaly first half of year and a negative seasonal anomaly in second half of year; thus, the corresponding layer thickness ratio varies slightly in the seasonal cycle. The mean ratio α is approximately 0.28 for the 24.25^{o}N section. Since the meridional pressure gradient term is one order of magnitude larger than the local meridional wind stress (Fig. 3), the meridional flow through the Taiwan Strait is primarily driven by the meridional pressure gradient force set up by the basin-scale zonal wind stress.

4.1. Taiwan Strait Warm Current

The seasonal cycle of the total volume transport of TSWC (integrated from surface to bottom, hereafter TSWCT) along 24.25^{o}N and the forcing terms, including local wind stress and pressure gradient term, are given in Fig. 8. The TSWCT has a strong seasonal cycle with a minimum (0.46 Sv) in winter and a maximum (1.71 Sv) in summer (Fig. 8a). The annual mean volume transport of 1.04Sv is smaller than that with a value on the order of 2Sv diagnosed from observations (Fang et al., 2001;

Wang et al., 2003), but it is consistent with the previous numerical study result of 1.09Sv by Wu and Hsin (2005). The current data obtained from shipboard instruments are generally representative of the state under relatively calm weather conditions, and this may be the main reason that results from observations might overestimate the winter volume transport (Guan and Fang, 2006).

The local meridional wind stress averaged in the box across the Taiwan Strait (117.75^{o}E-120.75^{o}E, 23.75^{o}N-24.75^{o}N) plays a minor role in regulating the seasonal cycle of the TSWCT. In fact, local meridional wind stress is southward for most time of the annual cycle, except in summer. The southward wind reaches its annual maximum in November, dashed line in Fig. 8b. In comparison, TSWCT is always northward, with the annual maximum in July and the annual minimum in November, Fig. 8a. Thus, the monsoon system works as a force against the current through the Taiwan Strait for most part of the annual cycle, with the exception for the summer season when the local wind stress is northward and it works as a minor direct driver. TSWCT often flows against local wind, and this phenomenon has been documented thoroughly by many investigators, in particular Guan (2002) and Guan and Fang (2006). However, for a long time the dynamical nature of this counter-wind current had not been examined thoroughly.

Two stations, P1 and P2, are selected, where the meridional pressure gradient built up by the basin-scale zonal wind stress can be used to estimate the pressure difference between the southern and northern tips of the Taiwan Island, Fig. 5. A northward pressure gradient force between P1 and P2 should help to maintain a

northward current, in consistence with the annual mean flow direction of the Taiwan Warm Current.

On seasonal cycle time scale, the pressure gradient term calculated from Eq. 2 is maximum in winter and minimum in summer; thus, the pressure gradient term has a phase opposite to that of the TSWCT (Fig. 9b, thin solid line). It is clear that on seasonal time scale, the pressure term cannot be used as the force directly controlling the current. However, this is not a surprise, and we acknowledge that the pressure gradient term cannot explain the seasonal variations due to the fact that the time scale for the reduced gravity model to be valid is determined by the time required for the first baroclinic Rossby wave to move across the basin, which is much longer than the seasonal time scale.

On interannual and decadal time scales, the roles of different forcing terms played in regulating TSWCT are discussed as follows. Three terms are identified and compared, including the pressure gradient term between P1 and P2, the net forces term $F = -\alpha P_y + \tau^y_{shelf}$ and the Kuroshio transport (total integration from 119.25^{o}E to 122.25^{o}E along 21.25^{o}N).

Recent study by Yang (2007) has been focused on the role played by the Kuroshio transport. Accordingly to his argument, the pressure difference between the southern and northern strait is set by friction associated with the current of Kuroshio. We postulate that the corresponding pressure gradient term can be obtained from an inviscid model, which regulates flow outside the thin frictional boundary layer around

the island. In our model, the meridional pressure gradient is due to the basin-scale circulation, or the so-called far field in boundary layer theory, and it can be calculated as the meridional gradient of zonal wind stress integrated from the western boundary to the eastern boundary in the open ocean. Although these two approaches are dynamically linked, our scheme gives a simple and direct way to explore the variability of the TSWC on interannual to decadal time scales. Furthermore, our analysis is independent of the frictional parameterization associated with the western boundary current. In addition, our argument relies on the semi-geostrophy assumption for the western boundary current. In fact, western boundary current at this latitude can be treated as an inertial boundary current, i.e., for a model with zero friction at this latitude band or even for the case with no island our index is still applicable.

After the band-pass filtering, the interannual variability with 2-8yr signals is extracted, Fig. 9. The maximum correlation coefficient between the pressure gradient term and the TSWCT is 0.42, with the pressure gradient term leading by 3 months (Fig. 9a). The correlation coefficient between the TSWCT and the Kuroshio transport is also very high with the maximum coefficient 0.53 occurring when the Kuroshio transport leading by 4 months (Fig. 9b, thin curve & shaded curve). The correlation analysis discussed above indicated that on interannual time scale the Kuroshio transport can lead to variability of the TSWC. There is no direct relationship between the pressure gradient term and the Kuroshio transport, and a maximum correlation coefficient between them is 0.15 only, occurring with zero-lag (Fig. 9a curve & Fig. 9b thin curve).

The net force term F (Eq. 6) combining the pressure gradient term and local meridional wind stress is also described in Fig. 9b (bold curve). The maximum correlation coefficient between the net force term and the TSWCT can reach to 0.56 with 3 months leading (Fig. 9b, bold curve & shaded curve), which is higher than that between the pressure gradient term and TSWCT, 0.42 (Fig. 9a, bold curve & shaded curve). The interannual variability of the net force term is mainly controlled by the pressure gradient term, with a high correlation coefficient, 0.81 between them (Fig. 9a curve & Fig. 9b bold curve).

The decadal variability of the pressure gradient term, Kuroshio transport and TSWCT is shown in Fig. 10. Although the zero-correlation coefficient between the pressure gradient term and the TSWCT is only 0.34 (Fig. 10a), it can reach to 0.77 between the net force term and the TSWCT with zero-lag (Fig. 10b, bold curve & shaded curve). The correlation coefficient between net force term and pressure gradient term is 0.56 (Fig. 10a curve & Fig. 10b bold curve), and the correlation coefficient between net force term and meridional wind stress can reach to 0.70.

On decadal time scale, the Kuroshio transport does not seem to play a dominant role in regulating the TSWCT; the zero-lag correlation coefficient between them is quite small, and it is 0.33 only (Fig. 10b, thin curve & shaded curve). Although the maximum correlation coefficient between the Kuroshio transport and TSWCT can reach to 0.55, it occurs only when Kuroshio transport lag TSWCT by 72 months.

The correlations between different forcing terms for the interannual/decadal time scale are summarized in Fig. 11. It is quite interesting to note that the Kuroshio Current and the net force term both play important role on interannual/decadal variability of the TSWC. This nearly independence between these two forcing terms is consistent with our analysis in Part I. Basically, the meridional pressure term is a simple meridional gradient of the zonal wind stress integrated from the western to eastern boundaries, and there is no Rossby wave delay term involved. On the other hand, the transport of the western boundary current (Eq. 15', part I) includes contributions due to zonal wind stress integral and the Ekman pumping term which involves the integration of the Rossby wave delay term. As discussed in part I, these two terms have rather different time variability.

For the interannual time scale, the correlation between the pressure gradient term and the Kuroshio transport is 0.15 only with zero lag (Fig. 11a). It is also interesting to note that their performance is different for different time period. For example, the Kuroshio transport cannot explain variability of TSWCT for the period of 1970-1976, but the net force term matches the TSWCT very well in this period. For the decadal time scale their correlation coefficient is -0.09 with a zero-lag (Fig. 11b). Therefore, they are really independent forcing terms for the TSWCT. It is worthwhile to notice that, although the phase correlation between the local wind stress and the TWCT is higher than that of the pressure gradient term on both interannual and decadal time scale (Fig. 11a & Fig. 11b), the local wind forcing is actually working as a drag for most of the time, as shown in Fig. 3.

4.2. The competition of these two forces along the P-N section

As shown in Fig. 5, the mean ocean current at 5m depth along the 28°N section off coast simulated in the SODA data also exist a strong northeastward current against the local surface wind forcing which disappears at depth of 96.92m in SODA datasets; and this current is called TWC in Chinese study, and it is called Kuroshio separation in Japanese literatures.

The 28.75°N section between 124.25°E and 126.25°E is chosen to determine the off coast volume transport of the TWC (hereafter, TWCT), as shown in Fig. 5, where this section is denoted as Section B, which has two maximum northward velocity centers at the depth of 30m and 75m. The pressure gradient term between P3 and P4, and the local wind stress averaged in box (124.25°E-126.25°E, 28.25°N-29.25°N) are also estimated and combined to determine the net force term F. The specification of alpha was discussed in the previous section. The mean ratio α along 28.75°N is 0.32, which is similar to the value along 24.25°N (Fig. 7d).

On interannual time scale, the variability of the volume transport across section B is poorly linked to the pressure gradient term (Fig. 12a). When the TWCT leading the Kuroshio transport (total integration from 123.75°E to 127.25°E along 26.75°N) by 5 months, the maximum correlation coefficient occurs with 0.34 (Fig. 12b, shaded and thin curves). Similarly, there is no clear link between the net force term because the corresponding correlation coefficient is negative (Fig. 12b, shaded and heavy curves). Lack of correlation between the TSWCT and the meridional

pressure gradient term (and the net force term) is not surprising because it takes about 10 years for the first baroclinic Rossby waves to cross the basin. As a result, the reduced gravity model is not really valid for time scale shorter than 10 years.

On decadal time scale, the maximum correlation between the pressure gradient term and the TWCT can reach to 0.66 when the former leads by 81 months, and the zero-lag correlation coefficient is only 0.17 (Fig. 13a). The zero-lag correlation between the TWCT and the Kuroshio transport is -0.32, and the maximum occurs -0.45 when the transport of Kuroshio leading by 30 months (Fig. 13b, shaded and thin curves). The zero-lag correlation coefficient between the net force term and the TWCT is only -0.08, but it can reach to 0.63 when the force term leading by for about 81 months (Fig. 13b, shaded and heavy curves).

For comparison, the correlations between different terms are summarized in Fig. 11c and 11d. In particular, it is interesting to note that here again the correlation between the pressure gradient term and the Kuroshio transport is quite low, indicating that these two terms are dynamically nearly independent forcing terms.

The relationship between the Kuroshio transport and the pressure gradient term is also discussed here. On interannual time scales, their correlation coefficient can reach to 0.30 when the Kuroshio transport leading the pressure gradient term by 1 month (Fig. 11c). On decadal time scale, it is only 0.07 with zero-lag; and it can reach to 0.27 when Kuroshio transport leading by 56 months (Fig. 11d).

5. Summary and discussion

In this study we have re-examined the maintenance and regulation of the meridional circulation in the western coastal zone. Our framework is a combination of a reduced gravity model for the wind-driven circulation in the basin interior and the classical boundary layer theory. The meridional pressure gradient along the outer edge of the coastal zone set up by the wind-driven circulation in the basin interior can be used an a useful index to explore the circulation in the western coastal zone, such as the warm countercurrent through the Taiwan Strait.

Analysis of the SODA data confirmed that the meridional pressure gradient set up by the basin-scale circulation is indeed an important regulator for the meridional circulation in the western coastal zone. In fact, this meridional pressure gradient is much larger than the meridional wind stress over the strait; thus, it can overpower the southward local wind stress and produces a northward flow. In addition, data analysis indicated that the TWCT is also highly correlated to the transport of Kuroshio Current. This high correlation suggests that TWCT may have its upstream source linked to the branch of Kuroshio Current near the Luzon Strait. In fact, Kuroshio can send out a small branch which passes through the Luzon Strait and eventually feeds the Taiwan warm current.

Our analysis and the theory discussed in Part I shown that the meridional pressure gradient term and the Kuroshio transport are poorly correlated. This is also been confirmed through data analysis discussed above. Therefore, these two mechanisms can be treated almost as independent dynamical factors regulating the meridional circulation in the western coast of North Pacific.

Most importantly, we demonstrated the close connection between the meridional circulation in the western coastal zone and the zonal wind stress in the basin interior on the interannual/decadal time scale. This may shoot light on the connection of climate change of the basin-scale forcing and circulation and climate change over the western coastal zone.

It is to emphasize that although we have presented some seemingly convincing results in supporting our framework, it is obvious the circulation in the western coastal zone, in particular the counter-current, involves many complicated dynamical processes; thus, other mechanisms may exist, which are left for further study.

Acknowledgement : This study was supported by the National Natural Science Foundation of China through Grant 40806005 and partially supported under the SCSIO Grant SQ200814. We are grateful for the critical comments from Drs. K. H. Brink and S. J. Lentz on the early version of this manuscript.

References:

Brink, K.H., 1998: Deep-sea forcing and exchange processes. In *The Sea*, volume 10, K.H. Brink and A.R. Robinson, editors, J. Wiley & Sons, New York, 151-170.

Chuang W. S., 1986: A note on the driving mechanism of current in the Taiwan Strait. *J. Oceanogr. Soc. Japan*, **42**, 355-361.

Csanady, G. T., 1977: Reply. *J. Geophy. Res*., **82**, 1453.

Fang, G., B. Zhao, and Y. Zhu, 1991: Water volume transport through the Taiwan Strait and the continental shelf of the East China Sea measured with current meters. *Oceanography of Asian Marginal Seas*, K. Takano, Ed., Elsevier, 345–358.

Guan, B. X., 2002: Winter counter-wind current off the southeastern China coast. China Ocean University Press, Qingdao, 267 pp. (in Chinese).

Guan, B. X., and S. J. Chen, 1964: The Current systems in the near-sea area of China Seas. 85 pp. (in Chinese).

Guan, B. X., and G. H. Fang, 2006: Winter Counter-wind Currents off the southeastern China Coast: A Review. *J. Oceanogr.*, 62, 1-24.

Huang, R. H. and Q.-Y., Liu: Meridional circulation in the western coastal zone, Part I. Variability of off-shore thermocline depth and western boundary current transport on interannual and decadal time scales, manuscript submitted to *J. Phys. Oceanogr*.

Luyten, J. R., 1977: Scales of motion in the deep Gulf Stream and across the Continental Rise. *J. Mar. Res*., **35**, 49-74.

Ma, C., J. Y. Yang, D. X. Wu, and X. P. Lin, 2009: The Kuroshio extension: a leading mechanism for the seasonal sea-level variability along the west coast of Japan. *Ocean Dynamics*, doi: 10.1007/s10236-009-0239-9.

Su, J. L., and W. Wang, 1987: On the sources of the Taiwan Warm Current from South China Sea. *Chin. J. Oceanol. Limnol*., **5**, 299-308.

Yang, J. Y., 2007: An oceanic current against the wind: how does Taiwan Island steer warm water into the East China Sea? *J. Phys. Oceanogr.*, **37**, 2563-2569.

Wang, Y. H., S. Jan, and D. P. Wang, 2003: Transports and tidal current estimates in the Taiwan Strait from shipboard ADCP observations (1999-2001). *Estuar. Coast. Shelf. Sci.*, **57**, 193-199.

Wu, C. R., and Y. C. Hsin, 2005: Volume transport through the Taiwan Strait: A numerical study. *TAO*, **16**, 377-391.

Figure captions:

Fig. 1. Sketch of the interaction between the open ocean and the coastal circulation

Fig. 2: Sketch of the interaction between the open ocean gyre and the coastal circulation along the western boundary.

Fig. 3: The annual mean pressure gradient term (a); first term of net force with $\alpha = 0.25$ (b) and meridional wind stress term (c) along the western boundary in the Pacific. The positive values indicate the pressure gradient force and wind stress are northward. Unit: $N.m^{-2}$.

Fig. 4: The annual mean pressure gradient term (a); first term of net force with $\alpha = 0.15$ (b) and meridional wind stress term (c) along the western boundary in the Atlantic. The positive values indicate the pressure gradient and wind stress are northward. Unit: $N.m^{-2}$.

Fig. 5: The region of the theory applied. Depth contours are in meters. The mean ocean current in 5.01m (bold vectors) and wind stress (line vectors) are both over-plotted. The bold dashed-lines indicate the two sections we chosen to estimate the total volume transport. Section A: Taiwan Strait Current (117.75 ^{o}E-120.75^{o}E, 24.25^{o}N); section B: Taiwan Warm Current off coast (124.25^{o}E-126.25^{o}E, 28.75^{o}N). The two boxes are given to estimate the averaged local meridional wind stress across A and B sections respectively. The locations of the pressure gradient are estimated between the locations between station 1 (120.25^{o}E, 21.25^{o}N) and station 2 (121.75^{o}E, 25.75^{o}N), station 3 (125.25^{o}E, 27.25^{o}N) and station 4 (126.75^{o}E, 29.75^{o}N) separately.

Fig. 6: The mean temperature profile along 24.25°N (a) and 28.75°N (b). The layer thickness of the coastal ocean (h) is chosen to be a constant, which is set to 100m along section A and 112.3m in section B respectively. The main thermocline along the outer edge of the wind-driven gyre (H) is defined by the depth of 14°C isotherm, which locates in (123.25°E, 24.25°N) and (128.25°E, 28.75°N) respectively.

Fig. 7: The seasonal cycle of the thermocline depth along the outer edge of the wind-driven gyre locates at (a) 123.25°E, 24.25°N; (b) 128.25°E, 28.75°N; and the ratio of layer thickness of the coastal ocean and the thermocline depth (c) along 24.25°N and (d) 28.75°N respectively. In climatologically mean, the 14°C isotherm depth at station (123.25°E, 24.25°N) is approximately 361.5m, and it is approximately 350.2m at station (128.25°E, 28.75°N). The mean ratio α is approximately 0.28 and 0.32 for the 24.25°N and 28.75°N separately.

Fig. 8: The seasonal cycle of (a) total volume transport integrated from surface to bottom; (b) the force term of the local meridional wind stress averaged in the box across Taiwan Strait (dashed-line), pressure gradient term between the P1 and P2 (real line), and the net force term F (bold line). Positive values indicate northward.

Fig. 9: The normalized interannual variability of (a) pressure gradient term (real curve); (b) the Kuroshio transport integrated from 119.25°E to 122.25°E along 21.25°N (fine curve), the net force term (bold curve); and the TSWCT (shaded curve). The positive number in bracket denotes the curves leading the bar for n months, and negative value denotes lag.

Fig. 10: The normalized decadal variability of (a) pressure gradient term (real curve); (b) the Kuroshio transport (fine curve), the net force term (bold curve); and the Taiwan Strait transport (shaded curve).

Fig. 11: Correlation coefficients between different terms, the positive values in bracket denote the TSWCT/TWCT lagging: Panels a and b for the 24.25^{o}N section, and Panels c and d for the P-N section. Assume the sample number n=28, $t_\alpha = 2.056$, and the critical value of correlation coefficient $r_c = \sqrt{t_\alpha^2 / \left(n - 2 + t_\alpha^2\right)}$ =0.374. Hence, correlation coefficients larger than this critical value pass the significant level test.

Fig. 12: The normalized interannual variability of (a) pressure gradient term (real curve); (b) the Kuroshio transport integrated from 123.75^{o}E to 127.25^{o}E along 26.75^{o}N (fine curve), the net force term (bold curve); and the TWCT (shaded curve).

Fig. 13: The normalized decadal variability of (a) pressure gradient term (real curve); (b) the Kuroshio transport integrated from 123.75^{o}E to 127.25^{o}E along 26.75^{o}N (fine curve), the net force term (bold curve); and the TWCT (shaded curve).

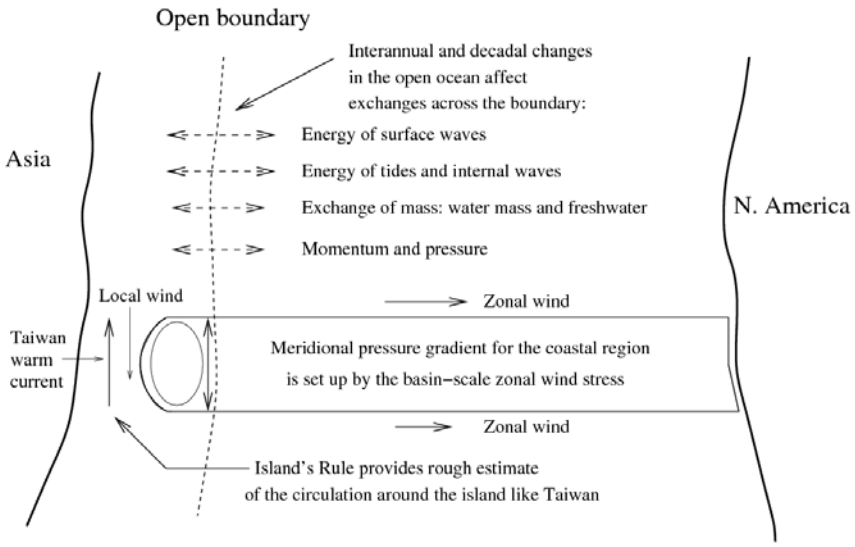

Fig. 1. Sketch of the interaction between the open ocean and the coastal circulation

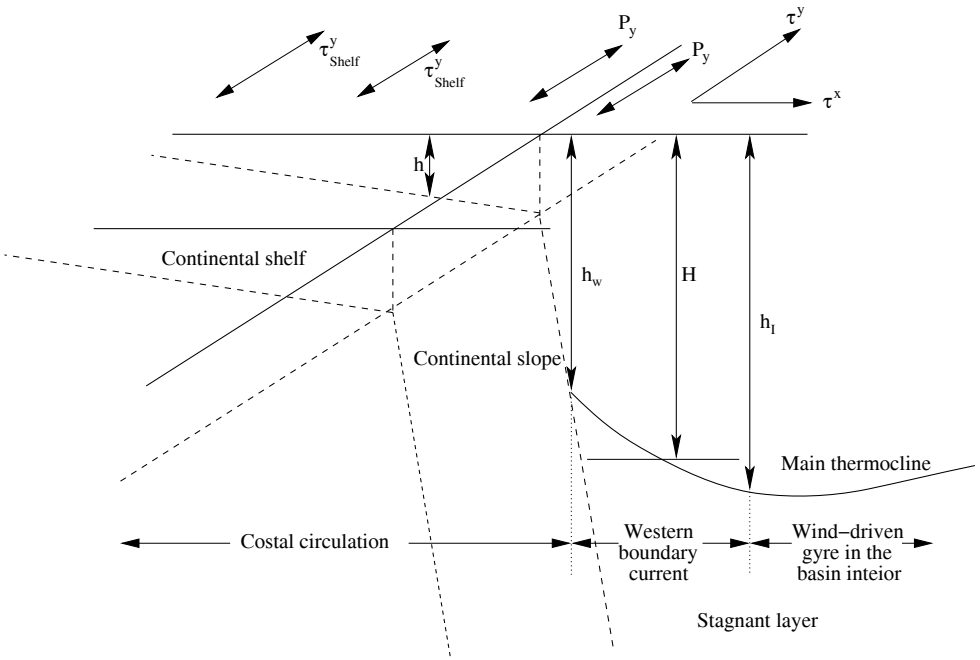

Fig. 2: Sketch of the interaction between the open ocean gyre and the coastal circulation along the western boundary.

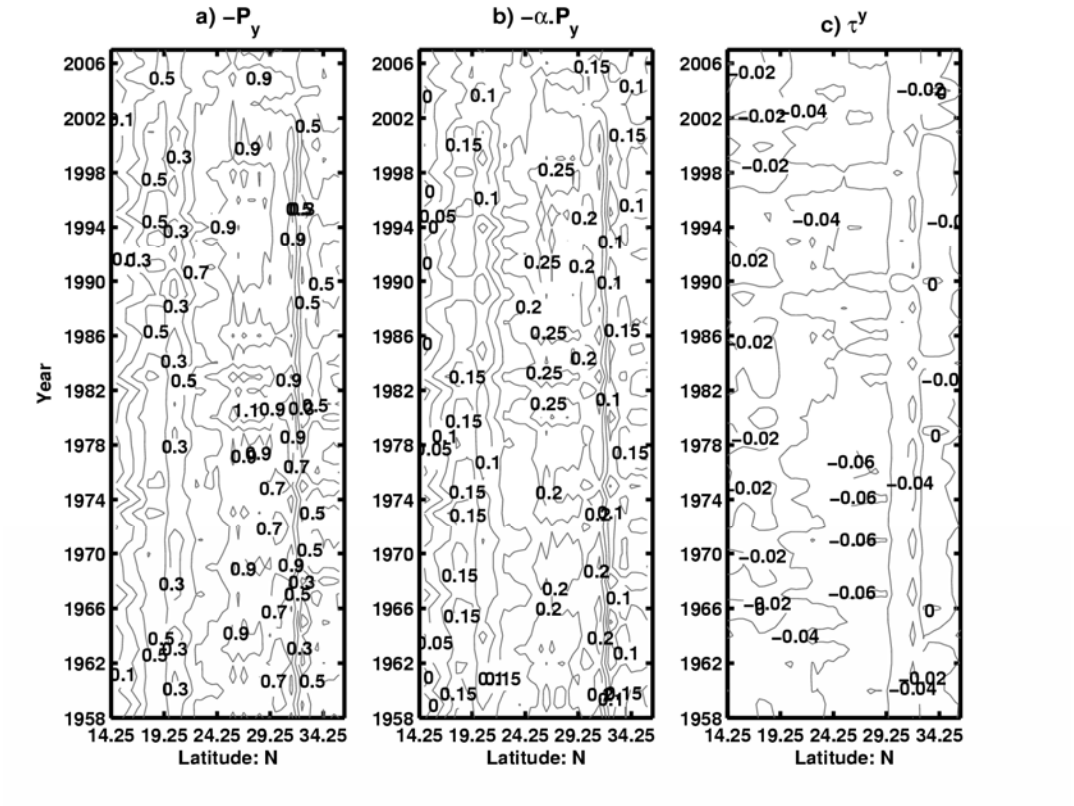

Fig. 3: The annual mean pressure gradient term (a); first term of net force with $\alpha = 0.25$ (b) and meridional wind stress term (c) along the western boundary in the Pacific. The positive values indicate the pressure gradient force and wind stress are northward. Unit: $N.m^{-2}$.

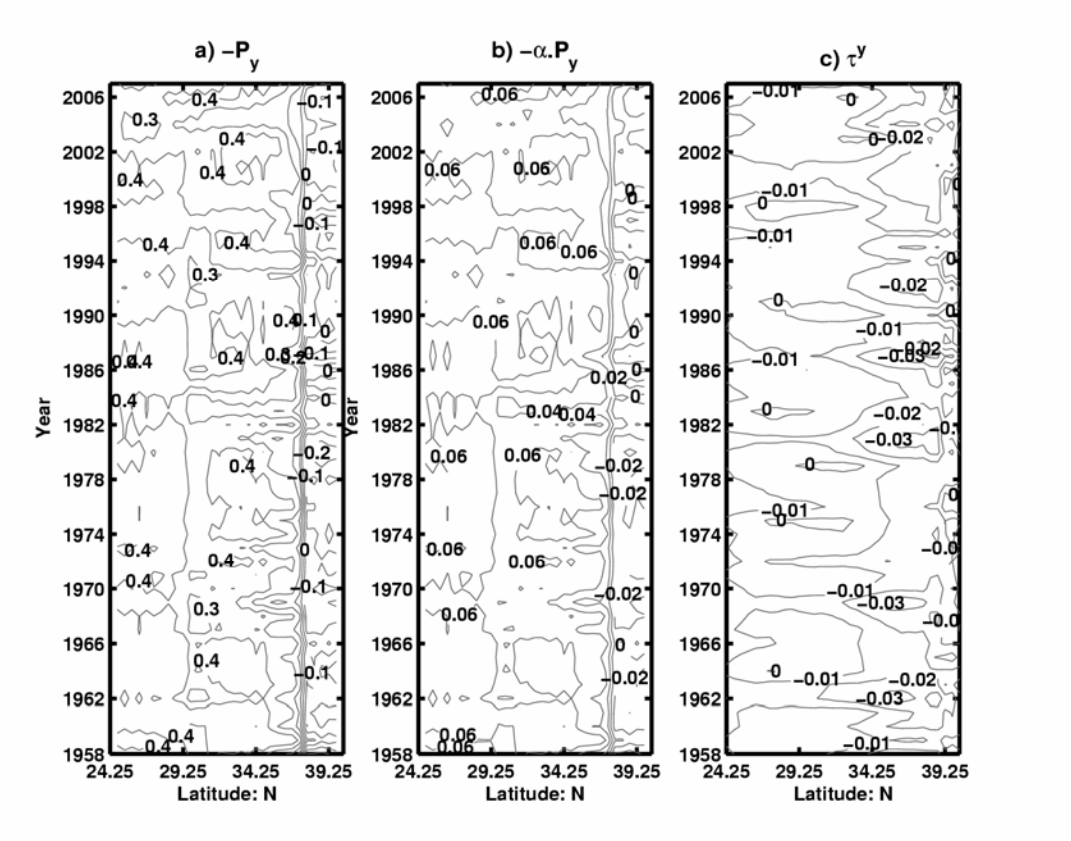

Fig. 4: The annual mean pressure gradient term (a); first term of net force with $\alpha = 0.15$ (b) and meridional wind stress term (c) along the western boundary in the Atlantic. The positive values indicate the pressure gradient and wind stress are northward. Unit: $N.m^{-2}$.

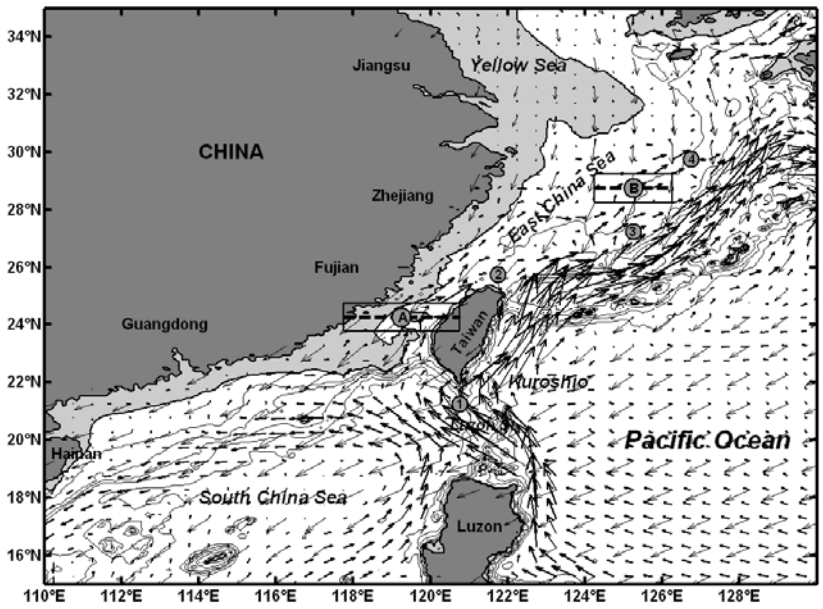

Fig. 5: The region of the theory applied. Depth contours are in meters. The mean ocean current in 5.01m (bold vectors) and wind stress (line vectors) are both over-plotted. The bold dashed-lines indicate the two sections we chosen to estimate the total volume transport. Section A: Taiwan Strait Current (117.75 ^{o}E-120.75^{o}E, 24.25^{o}N); section B: Taiwan Warm Current off coast (124.25^{o}E-126.25^{o}E, 28.75^{o}N). The two boxes are given to estimate the averaged local meridional wind stress across A and B sections respectively. The locations of the pressure gradient are estimated between the locations between station 1 (120.25^{o}E, 21.25^{o}N) and station 2 (121.75^{o}E, 25.75^{o}N), station 3 (125.25^{o}E, 27.25^{o}N) and station 4 (126.75^{o}E, 29.75^{o}N) separately.

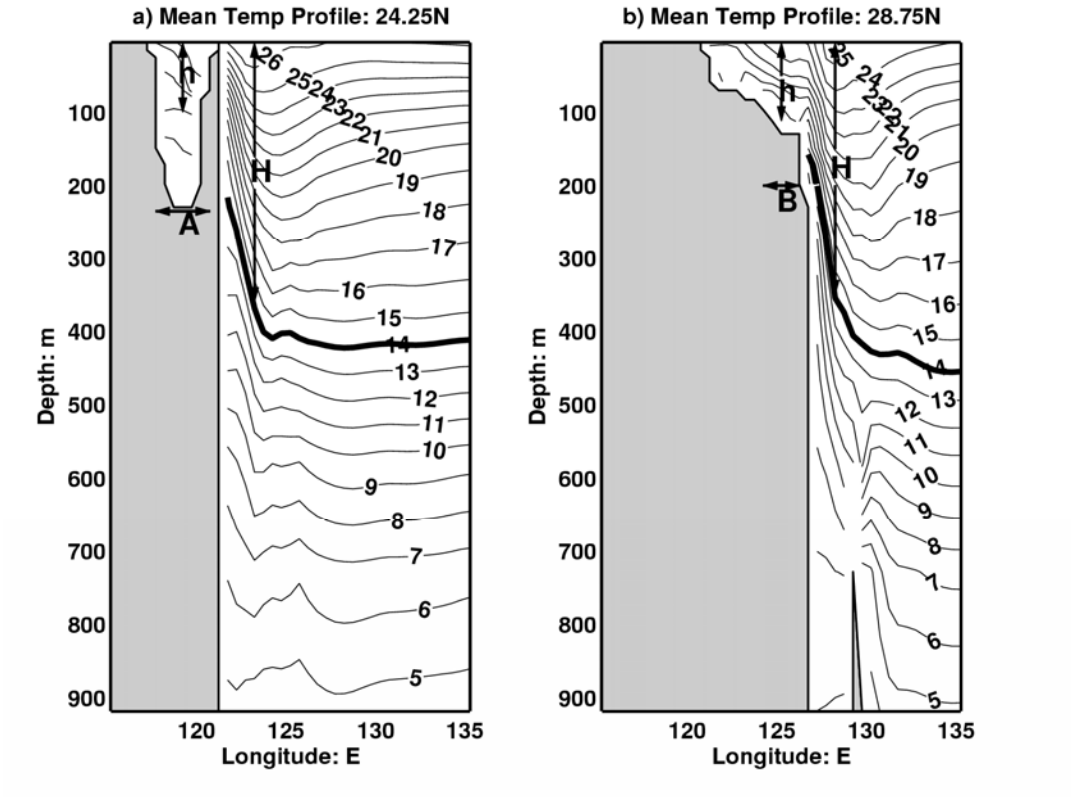

Fig. 6: The mean temperature profile along 24.25°N (a) and 28.75°N (b). The layer thickness of the coastal ocean (h) is chosen to be a constant, which is set to 100m along section A and 112.3m in section B respectively. The main thermocline along the outer edge of the wind-driven gyre (H) is defined by the depth of 14°C isotherm, which locates in (123.25°E, 24.25°N) and (128.25°E, 28.75°N) respectively.

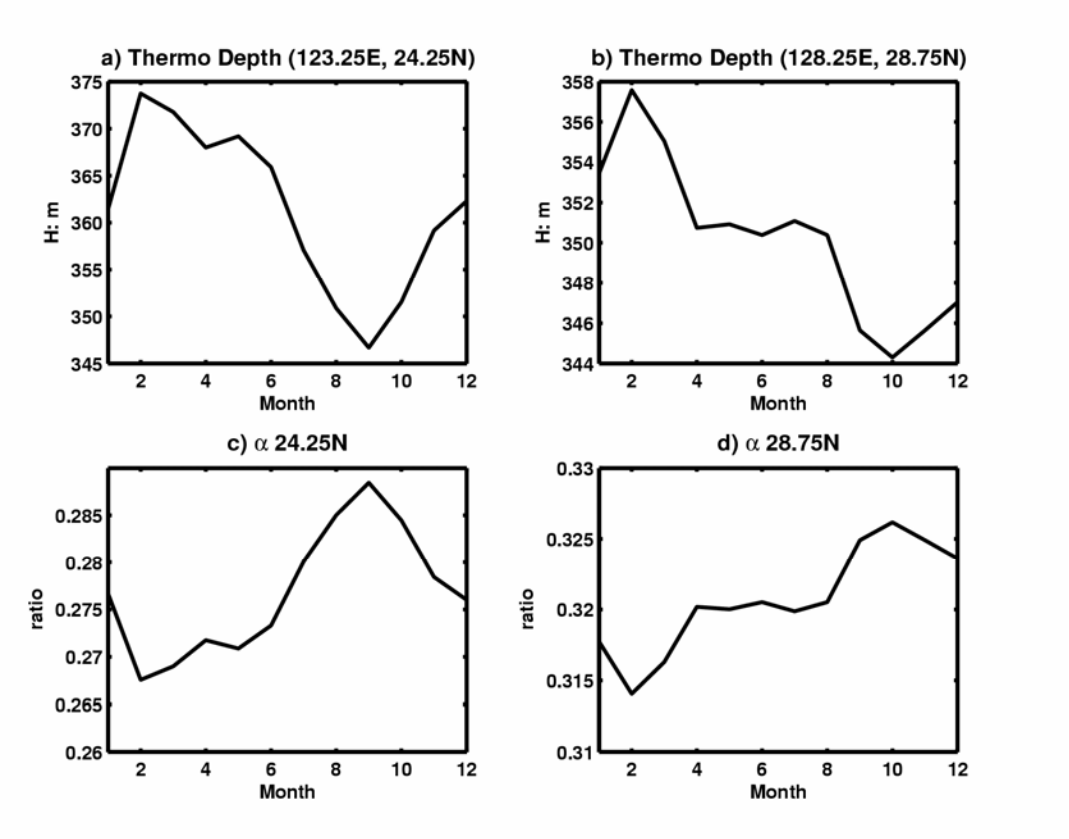

Fig. 7: The seasonal cycle of the thermocline depth along the outer edge of the wind-driven gyre locates at (a) 123.25^{o}E, 24.25^{o}N; (b) 128.25^{o}E, 28.75^{o}N; and the ratio of layer thickness of the coastal ocean and the thermocline depth (c) along 24.25^{o}N and (d) 28.75^{o}N respectively. In climatologically mean, the 14°C isotherm depth at station (123.25^{o}E, 24.25^{o}N) is approximately 361.5m, and it is approximately 350.2m at station (128.25^{o}E, 28.75^{o}N). The mean ratio α is approximately 0.28 and 0.32 for the 24.25^{o}N and 28.75^{o}N separately.

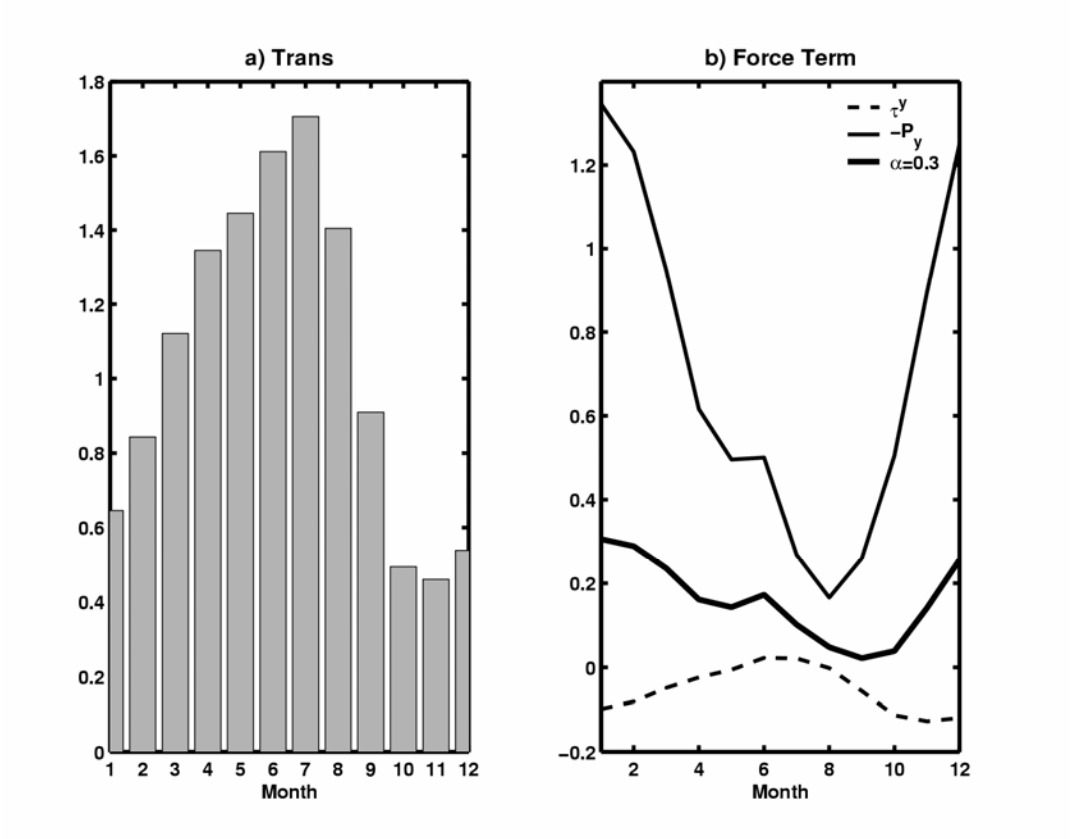

Fig. 8: The seasonal cycle of (a) total volume transport integrated from surface to bottom; (b) the force term of the local meridional wind stress averaged in the box across Taiwan Strait (dashed-line), pressure gradient term between the P1 and P2 (real line), and the net force term F (bold line). Positive values indicate northward.

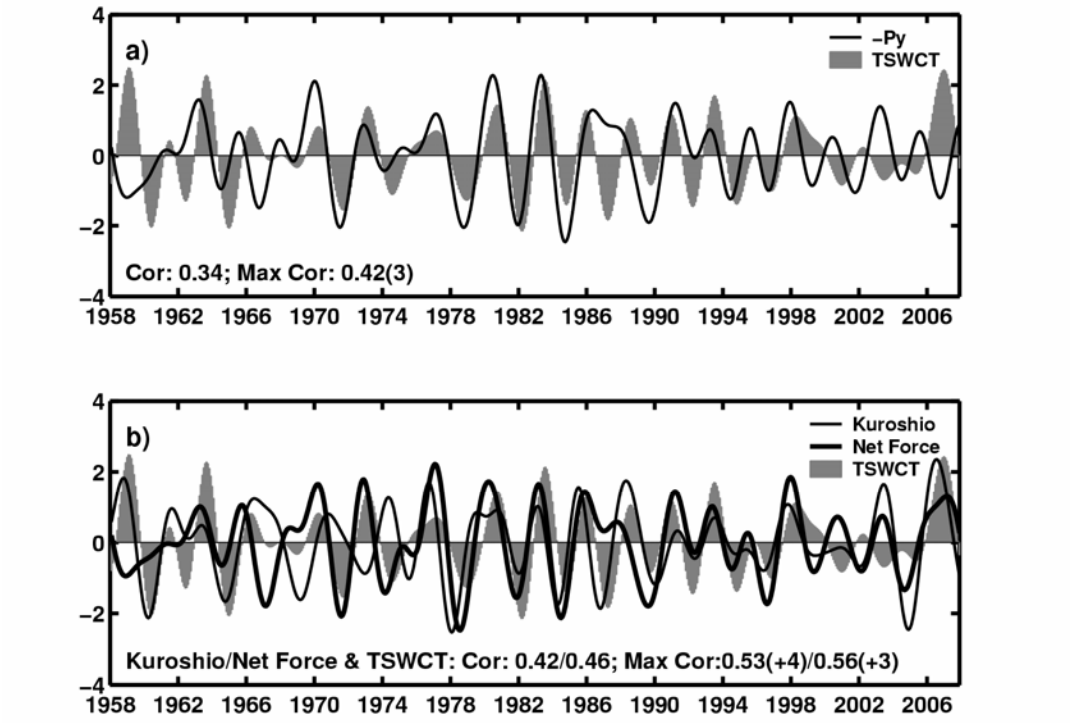

Fig. 9: The normalized interannual variability of (a) pressure gradient term (real curve); (b) the Kuroshio transport integrated from 119.25^{o}E to 122.25^{o}E along 21.25^{o}N (fine curve), the net force term (bold curve); and the TSWCT (shaded curve). The positive number in bracket denotes the curves leading the bar for n months, and negative value denotes lag.

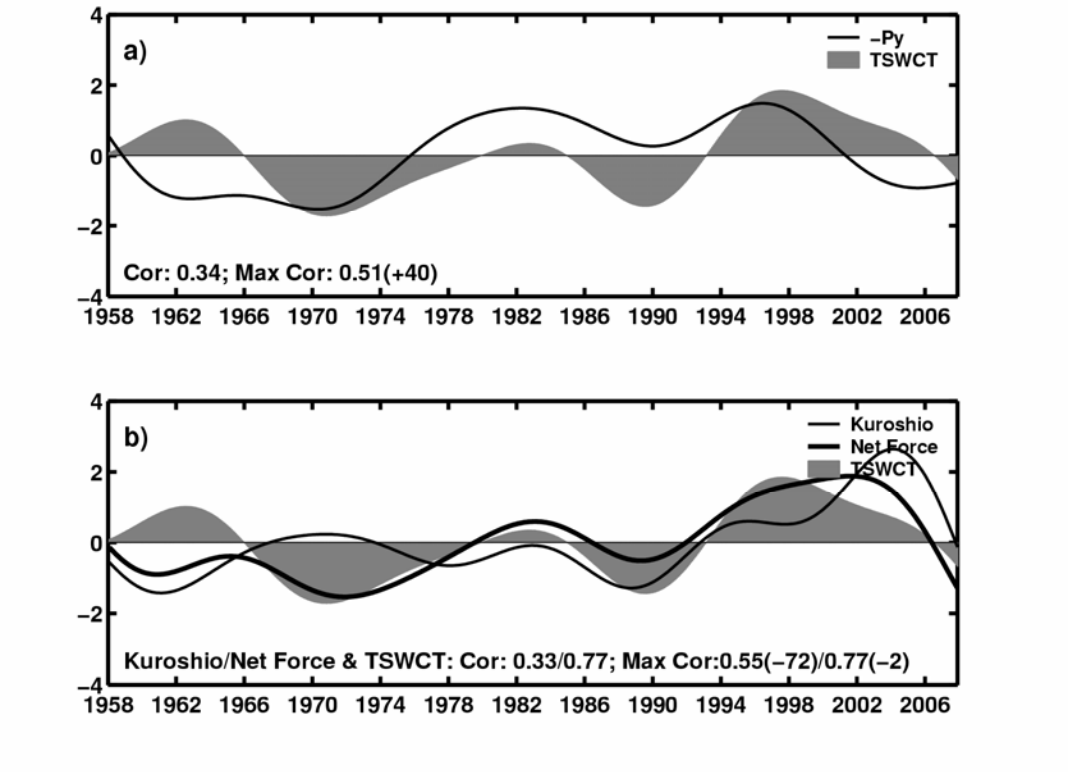

Fig. 10: The normalized decadal variability of (a) pressure gradient term (real curve); (b) the Kuroshio transport (fine curve), the net force term (bold curve); and the Taiwan Strait transport (shaded curve).

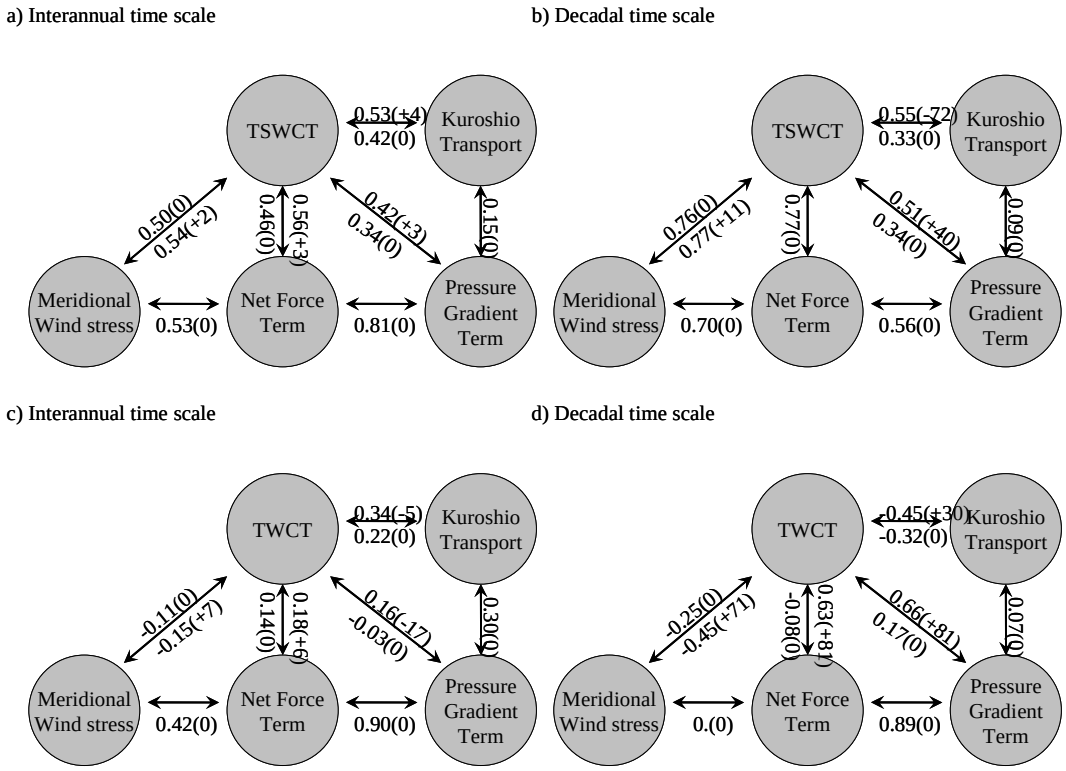

Fig. 11: Correlation coefficients between different terms, the positive values in bracket denote the TSWCT/TWCT lagging: Panels a and b for the 24.25°N section, and Panels c and d for the P-N section. Assume the sample number n=28, $t_\alpha = 2.056$, and the critical value of correlation coefficient $r_c = \sqrt{t_\alpha^2 / \left(n - 2 + t_\alpha^2\right)}$ =0.374. Hence, correlation coefficients larger than this critical value pass the significant level test.

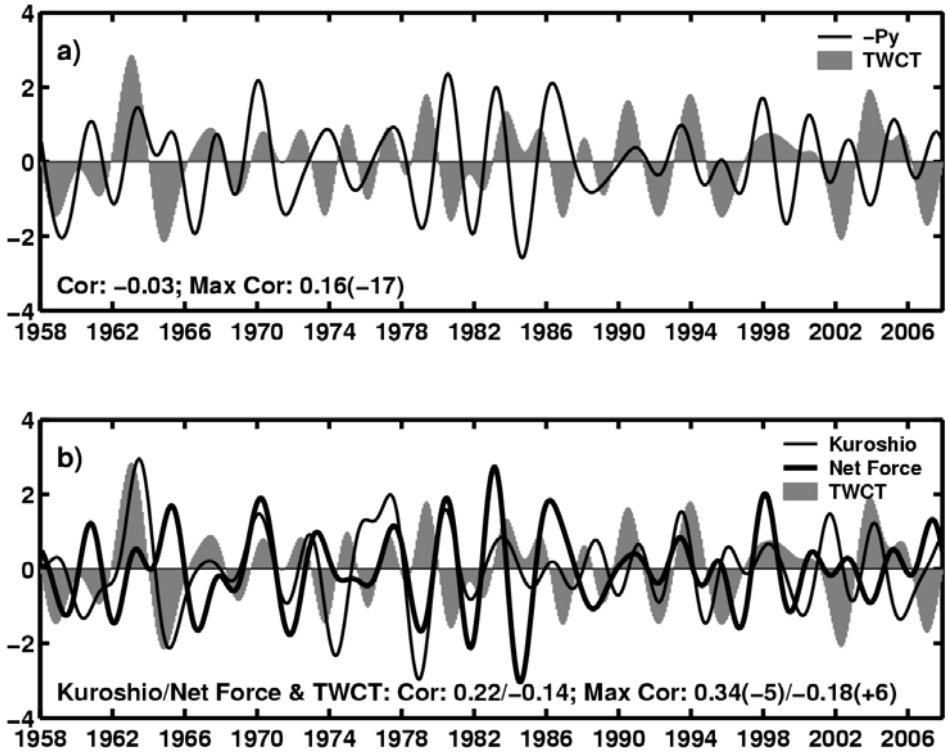

Fig. 12: The normalized interannual variability of (a) pressure gradient term (real curve); (b) the Kuroshio transport integrated from 123.75^{o}E to 127.25^{o}E along 26.75^{o}N (fine curve), the net force term (bold curve); and the TWCT (shaded curve).

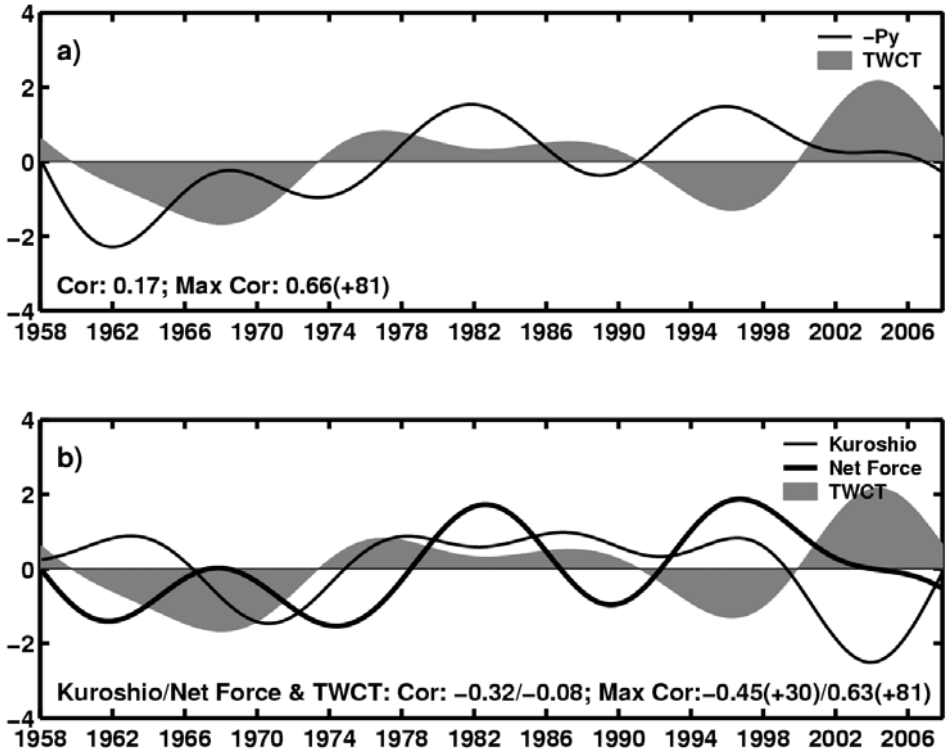

Fig. 13: The normalized decadal variability of (a) pressure gradient term (real curve); (b) the Kuroshio transport integrated from 123.75^{o}E to 127.25^{o}E along 26.75^{o}N (fine curve), the net force term (bold curve); and the TWCT (shaded curve).